HHS Public Access

Author manuscript

*ACS Chem Biol*. Author manuscript; available in PMC 2023 May 20.

Published in final edited form as:

*ACS Chem Biol*. 2022 May 20; 17(5): 1082–1091. doi:10.1021/acschembio.1c00925.

# Dark Dynamic Therapy: Photosensitization without Light Excitation Using Chemiluminescence Resonance Energy Transfer in a Dioxetane–Erythrosin B Conjugate

**Elyse M. Digby**,
Department of Chemical and Physical Sciences, University of Toronto Mississauga, Mississauga, Ontario L5L 1C6, Canada

**Matthew T. Tung**,
Department of Chemical and Physical Sciences, University of Toronto Mississauga, Mississauga, Ontario L5L 1C6, Canada

**Husain N. Kagalwala**,
Department of Chemistry, Center for Drug Discovery, Design, and Delivery (CD4), and Center for Global Health Impact (CGHI), Southern Methodist University, Dallas, Texas 75205-0314, United States

**Lucas S. Ryan**,
Department of Chemistry, Center for Drug Discovery, Design, and Delivery (CD4), and Center for Global Health Impact (CGHI), Southern Methodist University, Dallas, Texas 75205-0314, United States

**Alexander R. Lippert**,
Department of Chemistry, Center for Drug Discovery, Design, and Delivery (CD4), and Center for Global Health Impact (CGHI), Southern Methodist University, Dallas, Texas 75205-0314, United States

**Andrew A. Beharry**
Department of Chemical and Physical Sciences, University of Toronto Mississauga, Mississauga, Ontario L5L 1C6, Canada

## Abstract

Reactive oxygen species (e.g., singlet oxygen) are the primary cytotoxic agents used in the clinically approved technique photodynamic therapy (PDT). Although singlet oxygen has high

**Corresponding Author: Andrew A. Beharry** – Department of Chemical and Physical Sciences, University of Toronto Mississauga, Mississauga, Ontario L5L 1C6, Canada; andrew.beharry@utoronto.ca.

Supporting Information

The Supporting Information is available free of charge at https://pubs.acs.org/doi/10.1021/acschembio.1c00925.
Synthetic procedures, in vitro characterization data (absorbance, fluorescence, CL spectral comparisons, CL half-life data, response to ROS sensors, and NTR-CL-E1 activation), and *in cellulo* data (fluorescence images showing response to ROS sensors and intracellular uptake of probes, and cytotoxicity control data) (PDF)

Complete contact information is available at: https://pubs.acs.org/10.1021/acschembio.1c00925

The authors declare the following competing financial interest(s): A.R.L. declares a financial stake in BioLum Sciences, LLC.

DEDICATION

Dedicated to Prof. Eric T. Kool on his birthday.

potential to effectively kill tumor cells, its production via light excitation of a photosensitizer has been limited by the penetration depth and delivery of light in tissue. To produce singlet oxygen without light excitation, we describe the use of Schaap's chemiluminescent scaffold comprising an adamantylidene–dioxetane motif. Functionalizing this scaffold with a photosensitizer, Erythrosin B, resulted in spontaneous chemiluminescence resonance energy transfer (CRET) leading to the production of singlet oxygen. We show that this compound is cell permeable and that the singlet oxygen produced via CRET is remarkably efficient in killing cancer cells at low micromolar concentrations. Moreover, we demonstrate that protection of the phenol on the chemiluminescent scaffold with a nitroreductase-responsive trigger group allows for cancer-selective dark dynamic cell death. Here, we present the concept of dark dynamic therapy using a small cell-permeable molecule capable of producing the effects of PDT in cells, without light.

## Graphical Abstract

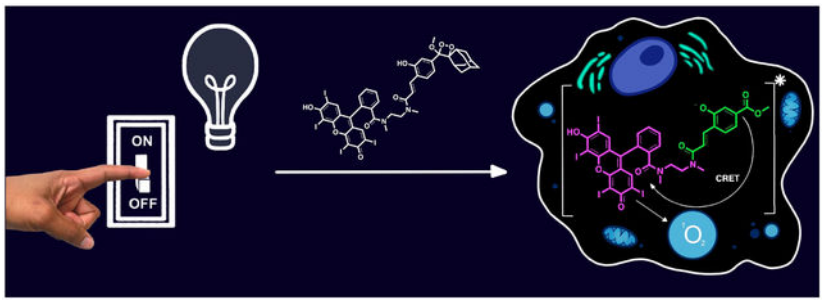


Photodynamic therapy (PDT) is a clinically approved cancer treatment that uses the combination of a photosensitizer (PS), molecular oxygen, and light (visible or near-infrared) to produce reactive oxygen species (ROS). Singlet oxygen, regarded as the most cytotoxic form of ROS,[1] is highly reactive and short-lived (~3.5 $\mu s$), such that once produced in a cancer cell, it will damage biomolecules nearby, leading to their dysfunction and ultimately causing cell death.[2,3] This unique cancer-killing mechanism (i.e., via oxidative stress) has made PDT capable of destroying tumors including their vasculature[1] and even do so in cases where patients have shown chemo-resistance.[4] However, the success of PDT is dependent on the production of singlet oxygen at the tumor site via light irradiation.[5] Since the penetration depth of light is limited to 1–5 mm beneath the skin,[6] the treatment of deeper cancers within the body requires invasive incisions or the feeding of fiber optics through natural openings in the body.[7,8] Even if delivery to the site is successful, light can still be scattered and attenuated by blood absorption, thereby limiting singlet oxygen to the outer linings of the target organs, translating to poor efficacy.[9] Thus, despite the ability of singlet oxygen to destroy tumor cells, its production requiring light excitation of a PS has limited its full therapeutic potential in treating cancers.

These challenges could, in principle, be addressed by applying PDT without external irradiation. This concept has been previously explored using bioluminescence resonance energy transfer (BRET).[10,11] An early example entailed conjugation of a small molecule PS to the protein transferrin, whereby in the presence of hydrogen peroxide, ferrous sulfate, and luminol, BRET activated the nearby PS causing cancer cell death.[12] Later studies

have employed a similar concept using the protein luciferase, either functionalized onto quantum dots containing a small molecule PS[13] or as a genetic fusion to protein-based PSs (e.g., miniSOG).[14,15] Although these studies have pioneered the concept of using luminescence to drive production of singlet oxygen without external light, its use is limited by the poor cellular uptake of proteins or genes, as well as the dependence of an exogenous enzyme that requires additional reagents to be added (e.g., luminol), which itself can induce cytotoxicity.[11,12] More recently, a hydrogen peroxide-triggered chemical excitation of a small molecule PS was developed.[16] Although singlet oxygen was produced without irradiation, cancer cell death was not demonstrated. Finally, the thermal decay of singlet oxygen release from 2-pyridone endoperoxides has been shown as a promising alternative to luminescence.[17,18] However, to date, cell killing has only been described for hypoxic conditions,[17] while normoxia required the addition of exogenous fluoride to enhance singlet oxygen release.[18,19] Moreover, 1,2-dihydropyridine endoperoxides have recently been demonstrated as efficient singlet oxygen storage and release compounds as well.[20]

As a proof-of-principle, we sought to develop a water-soluble, cell-permeable small molecule that can produce singlet oxygen without light excitation (i.e., dark dynamically) capable of killing cancer cells without requiring addition of exogenous agents. To this regard, we are using Schaap's chemiluminescent (CL) scaffold (Figure 1).[21–23] Comprising an adamantylidene–dioxetane motif, the Schaap CL probe can spontaneously disassemble to generate light upon formation of a phenolate (Figure 1A). Moreover, the scaffold has been shown to tolerate modifications at the *ortho* positions allowing for tuning of the CL wavelength and improving the CL brightness.[24] We note that although the removal of external irradiation reduces cancer selectivity compared to that achieved with PDT, we reasoned that the use of a scaffold that can readily permit activation by over-abundant analytes found in cancer cells could overcome this loss. To date, several groups have incorporated a variety of phenolate protecting groups that can be removed by analytes of interest (e.g., enzymes) as a means of detecting their abundance and for monitoring the release of chemotherapeutic agents.[24] However, the use of Schaap's probe to drive production of singlet oxygen as a potential therapeutic agent has not yet been demonstrated. We reasoned that the CL generated via disassembly of the Schaap probe can be used to activate an attached PS via chemiluminescence resonance energy transfer (CRET) (Figure 1A), whereby the resulting singlet oxygen produced can kill cancer cells.

To design a Schaap-based CL probe capable of producing singlet oxygen without light, we turned to the previously reported derivative containing an *ortho* methyl acrylate substituent.[25] We reasoned that hydrolysis of the methyl ester to a carboxylate will facilitate coupling to a PS via amide bond formation while still permitting disassembly and CL. For the PS, we selected Erythrosin B, a xanthene-based PS, which has broad absorption in the green region to permit efficient CRET with Schaap's derivative and possesses a high quantum yield of singlet oxygen production (0.63)[26] (Figure 1A). Due to the close proximity of Erythrosin B to the benzoate ester derivative (moiety responsible for CL), CRET is expected to generate singlet oxygen (Figure 1A).

## RESULTS AND DISCUSSION

Schaap's adamantylidene–dioxetane green-emitting probe precursor containing the methyl ester (**CL-OMe**) was synthesized using established methods[25,27] and then hydrolyzed using NaOH (Scheme S1). Commercially available Erythrosin B was modified with an amine linker (Scheme S2, compound **EryB-Linker**) and conjugated to Schaap's probe via amide bond formation followed by dioxetane formation to produce compound **CL-E1** (Figure 1A; Scheme S3). To aid in validating the expected mechanism of singlet oxygen production by **CL-E1**, we synthesized several control compounds (Figure 1B): First, to emphasize the importance of dioxetane breakdown for CRET, we employed the non-dioxetane version, **CL-E1a**, the synthetic precursor to **CL-E1** (Figure 1B; Scheme S3). To probe the role of the attached Erythrosin B dye, we synthesized the dioxetane composed of *ortho-N,N*-dimethylacrylamide (compound **CL-A**, Scheme S4), which lacks Erythrosin B, expected to breakdown to produce CL but not undergo CRET. To stress the requirement of a free phenolic OH for dioxetane breakdown and subsequent CRET/singlet oxygen production, we synthesized **CL-E2** (Scheme S5), whereby the phenolic OH was converted to a benzyl ether. Finally, to Schaap's CL scaffold, we conjugated the PS phenalenone (PN), whose absorption (340–440 nm) does not overlap with CL emission and thus can be used to further prove that the function of **CL-E1** occurs via CRET (compound **CL-PN** and Scheme S6). The final probes were purified by silica chromatography and/or RP-HPLC, and identities were confirmed by NMR and MS (see the Supporting Information). Stock solutions of all compounds were freshly prepared in DMSO prior to each experiment as under these conditions, the dioxetane samples are stable (Figure S1). The concentrations of **CL-E1** stock solutions were measured by UV–Vis spectroscopy in EtOH using the molar extinction coefficient of Erythrosin B, then aliquoted accordingly, dried down, and stored at −20 °C.

We first tested whether CRET occurs in **CL-E1**. Comparing the absorption and CL spectra of **EryB-Linker** and **CL-A**, respectively, we observed good spectral overlap (Figure S2), a requirement for CRET. When the absorbance and CL spectra were measured for **CL-E1** (PBS pH 7.4), a large degree of overlap was still observed although the CL maximum shifted relative to its unconjugated free form (i.e., **CL-A**), suggesting that CRET is still possible using the selected Erythrosin B dye and this Schaap derivative (Figure 2A). Note that although Erythrosin B is capable of fluorescence, its emission band ($\lambda_{em}$ = 550 nm, Figure S3) was not detected in these luminescence measurements, which we hypothesize is due to its low fluorescence quantum yield ($\Phi_f$ = 0.08).[26] Moreover, the slight shoulder in the absorbance spectrum of **CL-E1** at 600 nm is possibly due to the presence of some aggregated species in aqueous conditions, since in organic solvents like methanol, we do not observe the same shoulder (Figure S4). We next measured the CL half-life of **CL-E1** in PBS pH 7.4 at 37 °C. We observed a half-life ~1.5× shorter compared to that of **CL-A**, which contains no Erythrosin B (i.e., 10 ± 1 min versus 15 ± 3 min, respectively) (Figures 2B and S5). Moreover, **CL-PN** had a measured half-life of 16 ± 2 min (Figure S5), comparable to that of **CL-A**. We hypothesize that the observed small difference in half-lives is likely due to changes in the rate-limiting step (i.e., electron transfer from the phenolate to the dioxetane).[28] Both **CL-E1a** and **CL-E2** do not show any CL, which is expected, given their inability to breakdown (Figure S5). We further characterized the photophysical properties of

**CL-E1** and control compounds **CL-A** and **CL-PN** by measuring their fluorescence emission spectrum (Figure S6).

We next measured the CL quantum yield in PBS pH 7.4 using **CL-OMe dioxetane** as a CL standard, where a lower quantum yield would suggest CRET if the CL scaffold is conjugated to a suitable acceptor dye. **CL-E1** ($\Phi_{CL}$ 0.02 ± 0.006%) was found to be 80-fold dimmer compared to **CL-A** ($\Phi_{CL}$ 1.60 ± 0.04%) lacking Erythrosin B. Moreover, **CL-PN** ($\Phi_{CL}$ 0.56 ± 0.02%), which contains poor spectral overlap (Figure S7), was only 2.8-fold dimmer compared to CL-A, consistent with CRET being inefficient as set out in our design. Thus, the lower CL brightness of **CL-E1** confirms that CRET occurs between Schaap's adamantylidene–dioxetane derivative and the selected PS Erythrosin B.

Since Erythrosin B is known to produce singlet oxygen via irradiation,[26] we sought out to determine whether the CRET in **CL-E1** results in ROS production. To determine this, we employed the general ROS sensor, 2′,7′-dichlorofluorescin ($DCFH_2$), which gets oxidized by ROS to 2′,7′-dichloro-fluorescein (DCF) to produce green fluorescence.[29] To a solution of 5 μM $DCFH_2$ in PBS pH 7.4 containing 5% DMSO, **CL-E1** was added from a DMSO stock to yield a final concentration of 10 μM; then, the fluorescence was recorded at 5 min intervals (with the cuvette kept in the dark between measurements) at 37 °C. We observed an increase in fluorescence with time with a plateau after ~40 min and a half-life of 13 min consistent with the measured CL lifetime/half-life of **CL-E1** (Figure 3A). As the production of DCF was monitored using 490 nm excitation light, we observed minimal light-induced ROS by direct excitation of Erythrosin B when using **EryB-Linker** compared to **CL-E1**, indicating that ROS is produced mostly dark dynamically during these measurements (Figure S8). After 40 min incubation with increasing concentrations of **CL-E1** (5–20 μM), we also observed a dose-dependent increase in ROS production (Figure 3B). Moreover, we observed minimal DCF fluorescence from **CL-E1a** and **CL-E2**, which cannot produce CL, and from **CL-A** and **CL-PN**, which although produce CL are both incapable of CRET (Figure 3C), thereby further confirming that **CL-E1** produces ROS dark dynamically.

To determine the type of ROS produced by **CL-E1**, we repeated the $DCFH_2$ experiments with **CL-E1** in the presence of a singlet oxygen specific scavenger, sodium azide ($NaN_3$, 10 mM).[30,31] We observed ~8-fold lower DCF fluorescence compared to **CL-E1** (Figure 3A), confirming that the type of ROS produced by **CL-E1** is singlet oxygen. We note that the singlet oxygen specific sensors, 9,10-anthracenediyl-bis-(methylene)dimalonic acid (ABDA) or 1,3-diphenylisobenzofuran (DPBF), did not show a response to up to 20 μM **CL-E1** (Figure S9). We hypothesize that this is due to the lower sensitivity of ABDA and DPBF trapping agents compared to $DCFH_2$ oxidation,[31,32] which have previously required high probe concentrations (~100 μM) and a high percentage of co-organic solvents to produce observable changes,[16] both of which are currently not achievable with **CL-E1** (i.e., solubility limitations and CL requiring aqueous solution). Singlet Oxygen Sensor Green did not show a response to **CL-E1** (Figure S9) but also did not respond to singlet oxygen produced by irradiating Erythrosin B (Figure S10), in contrast to $DCFH_2$ under the same conditions (Figure S10). Finally, we estimated the singlet oxygen efficiency produced by **CL-E1** by relating the fluorescence intensity of DCF to its concentration,

using commercially available DCF and its known extinction coefficient, to construct a calibration curve (Figure S11). Using this curve with the DCF intensities produced by **CL-E1** (5, 10, and 20 $\mu$M), we calculate a singlet oxygen efficiency of 3.6 ± 0.51% (see the Supporting Information and Figure S11). We note that this value is an underestimate since all singlet oxygen produced will not be captured by $DCFH_2$ due to its short lifetime in water (~4 $\mu$s).[31] In support of this, repeating the ROS experiments with **CL-E1** (10 $\mu$M) containing $D_2O$ (1:2 $D_2O$/PBS pH 7.4), known to increase the lifetime of singlet oxygen (40–69 $\mu$s),[31] led to an ~2-fold higher production of singlet oxygen compared to 100% PBS (Figure S12). Using the $\Phi_{CL}$ of **CL-A** and **CL-E1** and the singlet oxygen quantum yield of Erythrosin B, we calculate the theoretical efficiency of singlet oxygen production by **CL-E1** to be 0.95% (see the Supporting Information). However, this calculation assumes that the chemiexcitation yield in **CL-E1** is equivalent to $\Phi_{CL\text{-}A}$, but it may be higher due to rapid energy transfer from the excited phenolate to Erythrosin B in **CL-E1**, which would translate to a higher singlet oxygen efficiency. Precedent for rapid energy transfer via CRET has been observed with previously reported Schaap's fluorophore-conjugated probes, which have superior brightness.[27]

Given the ability of **CL-E1** to produce singlet oxygen without light excitation *in vitro*, we asked whether this could occur in cells. We incubated MCF7 cells with the cell-permeable 2′,7′-dichlorofluorescin diacetate ($DCFH_2$-DA) ROS sensor, which when oxidized and cleaved via intracellular esterases produces the green fluorescent product DCF.[29] After 10 min incubation with **CL-E1** (5 $\mu$M), green fluorescence could be readily observed over background with maximum signals produced at 40 min without washing between imaging time points (Figure S13). Performing the same experiment with **CL-E1** but using a different sample devoted to each time point and washing before imaging revealed that the highest intracellular ROS signals occur at 10 min; and after that time, we observed that the DCF product diffuses out of cells, consistent with previous reports employing this sensor[33,34] (Figure S13). The time-dependent increase in DCF production is consistent with the CL lifetime of **CL-E1** and confirms that although **CL-E1** has a CL half-life of only 10 min, a portion is still capable of permeating cells to generate measurable intracellular ROS. Given that an incubation time of 10 min produced maximum intracellular signals, to accurately compare **CL-E1** data with controls, the remaining experiments were conducted at this time point. At increasing concentrations of **CL-E1** (2.5–20 $\mu$M), we observe a dose-dependent increase in ROS production (Figure 4A,B). To confirm that singlet oxygen was the primary type of ROS being produced *in cellulo*, we coincubated MCF7 cells with **CL-E1** (5 $\mu$M) and the singlet oxygen quencher $NaN_3$ (10 mM). Compared to the cells incubated with **CL-E1** only (Figure 4C), the cells with the addition of $NaN_3$ produced weaker green fluorescence signals (Figure 4C). Control compounds (**CL-E1a**, **CL-E2**, **CL-A**, and **CL-PN**) lacking the ability to undergo CRET and the use of free **EryB-Linker**, all produced DCF signals similar to background from the $DCFH_2$ sensor alone (Figures S14 and S15), consistent with the in vitro experiments. Finally, to further demonstrate that the breakdown of the dioxetane is responsible for CRET and singlet oxygen production, we preincubated **CL-E1** (5 $\mu$M) in cell culture media for 10 or 40 min prior to addition to cells. We observed lower DCF fluorescence for the **CL-E1** sample preincubated for 10 min and very minimal DCF signals for the 40 min preincubated sample (Figure 4D), both results being consistent with

the half-life of **CL-E1** and the time-dependent requirement for singlet oxygen production. To ensure that this result is not uniquely specific to MCF7 cells, we also tested for ROS production by **CL-E1** in A549 lung cancer cells and observed strong DCF signals in the cells incubated with **CL-E1** (5 $\mu$M) compared to minimal green fluorescence for those containing **CL-E1** in the presence of $NaN_3$ (10 mM) and control probes **CL-E1a**, **CL-E2,** **CL-A**, and **CL-PN** (5 $\mu$M) (Figures S16 and S17).

To complement the above ROS imaging experiment, we imaged the fluorescence from both the CL moiety for the expected benzoate ester product ($\lambda_{ex}$ 400 nm and $\lambda_{em}$ 560 nm) and Erythrosin B ($\lambda_{ex}$ 509 nm and $\lambda_{em}$ 544 nm) from **CL-E1** using fluorescence microscopy. Both compounds, though dim, have been previously fluorescently imaged *in cellulo*.[35,36] We incubated MCF7 cells with 10 $\mu$M **CL-E1** and collected images every 10 min with no washes. A time-dependent increase in the fluorescence of the benzoate product after dioxetane breakdown was observed with maximum signals occurring after 20 min of incubation and no difference between 20 and 60 min, consistent with the measured CL lifetime (Figure 5A,B). In contrast, the fluorescence by Erythrosin B, expected to be sustained before and after dioxetane breakdown, did not show any statistically significant differences between 10 and 60 min (Figure S18). Thus, the increases in the fluorescence of the benzoate product with time and the maintained fluorescence of Erythrosin B are consistent with dioxetane breakdown of **CL-E1** inside cells. It is worth noting that the observed intracellular fluorescence of Erythrosin B within 10 min and the ability to image the benzoate product intracellularly without washes suggest that **CL-E1** having a CL half-life of 10 min is able to permeate cells rapidly to produce intracellular ROS. To ensure that the yellow fluorescence from **CL-E1** is due to the production of its corresponding benzoate ester, we repeated the experiment in MCF7 cells using **CL-E2** (10 $\mu$M), which contains Erythrosin B but produces no CL, hence no benzoate ester fluorophore. We observed fluorescence comparable to background in the yellow channel used to image the benzoate ester, while maintained green fluorescence from Erythrosin B was at similar intensities to that of **CL-E1** (Figure S19). Finally, the fluorescence from Erythrosin B of **CL-E1** with the fluorescence from the benzoate product after 30 min incubation showed good overlay with signals in the cytosol (Figure 5C) with some signals in the nucleus (Figure 5D).

Finally, we asked whether the amount of singlet oxygen produced from **CL-E1** was sufficient to kill cancer cells. We incubated MCF7 cells with increasing concentrations of **CL-E1** (0.5–64 $\mu$M) at 37 °C overnight and then assayed for viable cells using a standard MTT assay. We observed a dose-dependent decrease in cell viability with a relative $IC_{50}$ = 14 ± 2 $\mu$M (Figure 6) (note that at concentrations >64 $\mu$M, **CL-E1** exhibits solubility issues). In contrast, incubation with all control compounds (**CL-E1a**, **CL-E2**, **CL-A**, and **CL-PN**) under the same concentration range resulted in viable cells (Figure 6), consistent with their inability to produce singlet oxygen. The lack of cytotoxicity observed from **CL-E1a** and **CL-E2** suggests that the **CL-E1** scaffold itself is not simply cytotoxic, since both control compounds contain all main components of **CL-E1** except the dioxetane functionality (**CL-E1a**) or a free phenolic OH (**CL-E2**). Furthermore, the lack of cytotoxicity observed by **CL-A** and **CL-PN** demonstrates that the dioxetane breakdown products (i.e., the benzoate and adamantyl ketone moieties) are not the cause of cell death by **CL-E1**, and no death

is exerted specifically by **CL-PN**, which is capable of CL, further emphasizing that CRET is required in **CL-E1** to cause cell death. To further confirm that cytotoxicity was due to intracellular ROS production by **CL-E1**, we preincubated **CL-E1** for 40 min in cell culture media and then added the media containing broken down **CL-E1** to cells for overnight incubation. We observed minimal cell death (Figure 6), consistent with the lack of intracellular ROS-produced post-dioxetane breakdown (Figure 4D) and confirming that the dioxetane breakdown products from **CL-E1** are not the cause of cytotoxicity. Finally, we confirmed ROS or specifically singlet oxygen as the primary cytotoxic agent and cause of cell death exerted by **CL-E1** by incubating cells with **CL-E1** in the presence of $NaN_3$ (10 mM), which led to an increase in the number of viable cells (Figure 6). No cytotoxicity from $NaN_3$ was observed in MCF7 cells up to 10 mM (Figure S20). Overall, CRET-induced singlet oxygen production from **CL-E1** is capable of killing cancer cells.

To further elucidate the mechanism of cell death, we incubated MCF7 breast cancer cells with **CL-E1** (32 $\mu$M) and then added Annexin V-FITC and propidium iodide (PI) to cells. Annexin V-FITC binds phosphatidylserine that gets translocated to the outer cell membrane in cells undergoing apoptosis, while PI is a DNA-intercalating fluorophore that can only enter cells undergoing necrosis once their cell membrane is compromised.[37] After incubation with **CL-E1**, we observed bright red nuclear signals from PI with time and minimal green fluorescence suggesting that **CL-E1** kills MCF7 cells via necrosis (Figures 7 and S21).

As a proof-of-principle, to demonstrate that **CL-E1** can be activated enzymatically to produce singlet oxygen in a specific tumor cell line, we masked the phenol on the CL scaffold with a 4-nitrobenzyl group, a commonly employed trigger group for nitroreductase (NTR)-responsive probes,[38–40] including a recent CL probe constructed via Schaap's scaffold.[41] NTR's mechanism of action is to reduce nitro groups to amines in the presence of nicotinamide adenine dinucleotide (NADH).[42] We hypothesized that in the presence of NTR and NADH, reduction of 4-nitrobenzyl to 4-aminobenzyl would occur, followed by 1,4-elimination to generate the phenol on **CL-E1**, thereby triggering chemiexcitation, CRET, and then production of singlet oxygen (Figure 8A). To ensure that chemiexcitation was not the rate-limiting step, we modified **CL-E1** with a chlorine *ortho* to the phenol to lower the p$K_a$ of the phenol proton, which has been shown to result in faster dioxetane breakdown at physiological pH 7.4 once the phenolate is produced.[25] The synthesis required coupling between **EryB-Linker** and the previously reported **NTR-CL** probe[41] via amide bond formation to generate **NTR-CL-E1** (Scheme S9).

To test **NTR-CL-E1** for its ability to be acted upon by NTR, we used analytical RP-HPLC. We incubated a solution of **NTR-CL-E1** (50 $\mu$M) in PBS pH 7.4 with NTR (1.5 $\mu$M) and NADH (200 $\mu$M) overnight at 37 °C. Compared to **NTR-CL-E1** incubated with NADH only (elution time 41 min), the sample containing NTR showed the presence of a new peak at 37 min, which corresponds to the CL benzoate ester product at ~36% abundance (Figure S22). Repeating the experiment using a higher concentration of NTR (10 $\mu$M) produced more benzoate ester product (~56%) (Figure S22). We confirmed that an NTR substrate was required for CL phenol deprotection by repeating the experiments with **CL-E2** (i.e., lacking a nitro group), where no new peak was observed (Figure S23).

To determine if singlet oxygen was selectively produced upon NTR activation, we incubated **NTR-CL-E1** (10 $\mu$M) with NTR (1.5 $\mu$M) and NADH (200 $\mu$M), along with the general ROS sensor, $DCFH_2$ (5 $\mu$M), in PBS pH 7.4 for 24 h at 37 °C. The fluorescence of DCF was ~8-fold higher for **NTR-CL-E1** incubated with NTR and NADH, compared to **NTR-CL-E1** incubated with NADH alone (Figure 8B), suggesting that NTR is required for **NTR-CL-E1** to produce singlet oxygen. To further demonstrate that the removal of the trigger group is necessary for ROS to be produced, we repeated the experiments with **CL-E2** (10 $\mu$M) under the same NTR and NADH conditions, where minimal DCF fluorescence was observed with or without NTR (Figure 8B). To ensure that the increase in DCF fluorescence is not due to the production of nitro radical species that may be produced upon NTR reduction of nitro groups,[43] we conjugated 4-nitrobenzyl to the fluorophore resorufin (**4NB-Reso)** (Scheme S10). **4NB-Reso** is initially quenched in fluorescence ($\lambda_{ex}$ 472 nm) with an absorbance maximum at 450 nm. Incubation with NTR (0.5 $\mu$M) and NADH (100 $\mu$M) results in complete release of resorufin in 40 min (Figure S24). We measured ROS production from **4NB-Reso** under the same conditions used for **NTR-CL-E1** and observed a minimal increase in DCF fluorescence, thereby confirming that ROS from **NTR-CL-E1** is produced by CRET from the CL scaffold to Erythrosin B.

Finally, we set out to determine if **NTR-CL-E1** can produce ROS intracellularly and induce cancer cell death, dependent on NTR activity. To test this, we used triple-negative breast cancer cells, which have been modified to stably express NTR (MDA-MB231-NTR).[44] Incubating **NTR-CL-E1** (10 $\mu$M) and $DCFH_2$-DA (10 $\mu$M) in MDA-MB231-NTR cells for 45 min resulted in green DCF fluorescence (Figures 8C and S25). In contrast, incubation with native MDA-MB231 cells (i.e., containing no NTR) showed minimal DCF fluorescence (Figures 8C and S25), comparable to background fluorescence from the $DCFH_2$-DA sensor alone (Figure S25). Moreover, incubation of both cell lines with **NTR-CL-E1** and $DCFH_2$-DA for 90 min still showed ROS production at levels similar to the 45-min time point, suggesting that **NTR-CL-E1** is still being activated (Figure S25). Dosing **NTR-CL-E1** (0.1–32 $\mu$M) in both types of MDA-MB231 cell lines produced selective cytotoxicity in cells expressing NTR (Figure 8D). Higher potency was observed after 72-h (relative $IC_{50}$ = 1.9 ± 0.7 $\mu$M) versus 24-h incubation, which we hypothesize is due to slow activation of our probe by NTR, consistent with our in vitro and *in cellulo* ROS imaging data. In contrast, **CL-E2** induced no cytotoxicity, since it does not contain a substrate for NTR (Figure S26). Overall, these results demonstrate that **CL-E1** can be activated enzymatically in cancer cells when masking the phenol with a trigger group, thereby making dark dynamic therapy via CRET using Schaap's scaffold possible for tumor-selective applications. Although the potency of **NTR-CL-E1** to that of **CL-E1** cannot be compared as they were determined in different cell lines, generally, we do expect caged versions of **CL-E1** to have higher potencies due to potentially higher cell permeability and a larger fraction containing the intact dioxetane (i.e., cytotoxic form) entering cells. However, the slow-release mechanism (or production of ROS over a long timescale) of **NTR-CL-E1** by NTR activation could be weakening its full potential cytotoxicity, and hence, future constructs having faster uncaging release mechanisms may be desirable.

## CONCLUSIONS

In summary, we present a small molecule strategy to produce singlet oxygen in cells without the use of light excitation. Our strategy uses the CL resulting from the spontaneous breakdown of Schaap's dioxetane to excite a nearby PS causing production of single oxygen. Although our CRET strategy inherently produces lower amounts of singlet oxygen compared to PS irradiation as performed in PDT, we found that the amounts produced were sufficient to induce cancer cell death with low micromolar $IC_{50}$ values. We show that protecting the phenolic OH (**CL-E2**) abolishes the therapeutic properties of **CL-E1** and that installing an NTR-responsive trigger group can produce ROS and kill cancer cells in an NTR-dependent manner. Given the previous reports of Schaap's scaffold as a bioluminescence sensor,[24] it is likely that cancer selectivity can be achieved by installing additional trigger groups on the phenol group of **CL-E1** to serve as a replacement for the spatial selectivity exerted by light irradiation as achieved with classic PDT. Moreover, given the known derivatives of the dioxetane having different CL emission wavelengths,[24] the use of PS with different absorptions having near unity quantum yields may be used to potentially increase ROS production. Thus, the properties exerted by **CL-E1** represent a significant starting point for further investigations of dark dynamic therapy as a strategy to overcome the limitations of light excitation in conventional PDT. The versatility of Schaap's scaffold lends considerable promise to such explorations.

## Supplementary Material

Refer to Web version on PubMed Central for supplementary material.

## ACKNOWLEDGMENTS

A.A.B. acknowledges the support of the Government of Canada's New Frontiers in Research Fund (NFRF), [NFRFE-2020-00290]. A.R.L. acknowledges funding from the National Science Foundation (CHE 1653474) and the National Institutes of Health (NIGMS R15GM114792). The authors are grateful to R. Paulmurugan (Stanford) for providing us with MDA-MB-231 cells stably expressing NTR, and the authors thank A. Kaye for the generation of our table of contents graphic.

## REFERENCES

(1). Agostinis P; Berg K; Cengel KA; Foster TH; Girotti AW; Gollnick SO; Hahn SM; Hamblin MR; Juzeniene A; Kessel D; Korbelik M; Moan J; Mroz P; Nowis D; Piette J; Wilson BC; Golab J Photodynamic Therapy of Cancer: An Update. CA Cancer J. Clin 2011, 61, 250–281. [PubMed: 21617154]

(2). Baptista MS; Cadet J; Di Mascio P; Ghogare AA; Greer A; Hamblin MR; Lorente C; Nunez SC; Ribeiro MS; Thomas AH; et al. Type I and Type II Photosensitized Oxidation Reactions: Guidelines and Mechanistic Pathways. Photochem. Photobiol 2017, 93, 912–919. [PubMed: 28084040]

(3). Ogilby PR Singlet Oxygen: There Is Indeed Something New under the Sun. Chem. Soc. Rev 2010, 39, 3181–3209. [PubMed: 20571680]

(4). Spring BQ; Rizvi I; Xu N; Hasan T The Role of Photodynamic Therapy in Overcoming Cancer Drug Resistance. Photochem. Photobiol. Sci 2015, 14, 1476–1491. [PubMed: 25856800]

(5). Lovell JF; Liu TWB; Chen J; Zheng G Activatable Photosensitizers for Imaging and Therapy. Chem. Rev 2010, 110, 2839–2857. [PubMed: 20104890]

(6). Ash C; Dubec M; Donne K; Bashford T Effect of Wavelength and Beam Width on Penetration in Light-Tissue Interaction Using Computational Methods. Lasers Med. Sci 2017, 32, 1909–1918. [PubMed: 28900751]

(7). Mallidi S; Anbil S; Bulin AL; Obaid G; Ichikawa M; Hasan T Beyond the Barriers of Light Penetration: Strategies, Perspectives and Possibilities for Photodynamic Therapy. Theranostics 2016, 6, 2458–2487. [PubMed: 27877247]

(8). Simone CB 2nd; Friedberg JS; Glatstein E; Stevenson JP; Sterman DH; Hahn SM; Cengel KA Photodynamic Therapy for the Treatment of Non-Small Cell Lung Cancer. J. Thorac. Dis 2012, 4, 63–75. [PubMed: 22295169]

(9). van Straten D; Mashayekhi V; de Bruijn HS; Oliveira S; Robinson DJ Oncologic Photodynamic Therapy: Basic Principles, Current Clinical Status and Future Directions. Cancers (Basel) 2017, 9, 19.

(10). Ożóg Ł; Tabarkiewicz J; Aebisher D Chemiluminescence-Driven Dye Excitation for Dark Photodynamic Therapy. Eur. J. Clin. Exp. Med 2017, 15, 95–98.

(11). Magalhães CM; Esteves da Silva JCG; Pinto da Silva L Chemiluminescence and Bioluminescence as an Excitation Source in the Photodynamic Therapy of Cancer: A Critical Review. ChemPhysChem 2016, 17, 2286–2294. [PubMed: 27129132]

(12). Laptev R; Nisnevitch M; Siboni G; Malik Z; Firer MA Intracellular Chemiluminescence Activates Targeted Photodynamic Destruction of Leukaemic Cells. Br. J. Cancer 2006, 95, 189–196. [PubMed: 16819545]

(13). Kim YR; Kim S; Choi JW; Choi SY; Lee S-H; Kim H; Hahn SK; Koh GY; Yun SH Bioluminescence-Activated Deep-Tissue Photodynamic Therapy of Cancer. Theranostics 2015, 5, 805–817. [PubMed: 26000054]

(14). Proshkina GM; Shramova EI; Shilova ON; Ryabova AV; Deyev SM Phototoxicity of Flavoprotein MiniSOG Induced by Bioluminescence Resonance Energy Transfer in Genetically Encoded System NanoLuc-MiniSOG Is Comparable with Its LED-Excited Phototoxicity. J. Photochem. Photobiol. B Biol 2018, 188, 107–115.

(15). Kim EH; Park S; Kim YK; Moon M; Park J; Lee KJ; Lee S; Kim Y-P Self-Luminescent Photodynamic Therapy Using Breast Cancer Targeted Proteins. Sci. Adv 2020, 6, No. eaba3009. [PubMed: 32917700]

(16). Yesilgul N; Uyar TB; Seven O; Akkaya EU Singlet Oxygen Generation with Chemical Excitation of an Erythrosine–Luminol Conjugate. ACS Omega 2017, 2, 1367–1371. [PubMed: 30023632]

(17). Ayan S; Gunaydin G; Yesilgul-Mehmetcik N; Gedik ME; Seven O; Akkaya EU Proof-of-Principle for Two-Stage Photodynamic Therapy: Hypoxia Triggered Release of Singlet Oxygen. Chem. Commun 2020, 56, 14793–14796.

(18). Ucar E; Xi D; Seven O; Kaya C; Peng X; Sun W; Akkaya EU “Off-on” Switching of Intracellular Singlet Oxygen Release Under Biocompatible Conditions. Chem. Commun 2019, 55, 13808–13811.

(19). Qu M; Wu N; Jiang W; Wang L; Akkaya S; Akkaya EU Silyl-Naphthalene Endoperoxides as Switchable Sources of Singlet Oxygen for Bactericidal Activity. RSC Adv. 2021, 11, 19083–19087. [PubMed: 35478644]

(20). De Bonfils P; Verron E; Nun P; Coeffard V Photoinduced Storage and Thermal Release of Singlet Oxygen from 1, 2-Dihydropyridine Endoperoxides. ChemPhotoChem 2021, 5, 847–856.

(21). Schaap AP; Handley RS; Giri BP Chemical and Enzymatic Triggering of 1,2-Dioxetanes. 1: Aryl sterase-Catalyzed Chemiluminescence from a Naphthyl Acetate-Substituted Dioxetane. Tetrahedron Lett. 1987, 28, 935–938.

(22). Schaap AP; Chen T-S; Handley RS; DeSilva R; Giri BP Chemical and Enzymatic Triggering of 1,2-Dioxetanes. 2: Fluoride-Induced Chemiluminescence from Tert-Butyldimethylsilyloxy-Substituted Dioxetanes. Tetrahedron Lett. 1987, 28, 1155–1158.

(23). Schaap AP; Sandison MD; Handley RS Chemical and Enzymatic Triggering of 1,2-Dioxetanes. 3: Alkaline Phosphatase-Catalyzed Chemiluminescence from an Aryl Phosphate-Substituted Dioxetane. Tetrahedron Lett. 1987, 28, 1159–1162.

(24). Gnaim S; Green O; Shabat D The Emergence of Aqueous Chemiluminescence: New Promising Class of Phenoxy 1,2-Dioxetane Luminophores. Chem. Commun 2018, 54, 2073–2085.

(25). Green O; Eilon T; Hananya N; Gutkin S; Bauer CR; Shabat D Opening a Gateway for Chemiluminescence Cell Imaging: Distinctive Methodology for Design of Bright Chemiluminescent Dioxetane Probes. ACS Cent. Sci 2017, 3, 349–358. [PubMed: 28470053]

(26). Gandin E; Lion Y; Van de Vorst A Quantum Yield of Singlet Oxygen Production by Xanthene Derivatives. Photochem. Photobiol 1983, 37, 271–278.

(27). Hananya N; Eldar Boock A; Bauer CR; Satchi-Fainaro R; Shabat D Remarkable Enhancement of Chemiluminescent Signal by Dioxetane-Fluorophore Conjugates: Turn-ON Chemiluminescence Probes with Color Modulation for Sensing and Imaging. J. Am. Chem. Soc 2016, 138, 13438–13446. [PubMed: 27652602]

(28). Hananya N; Reid JP; Green O; Sigman MS; Shabat D Rapid Chemiexcitation of Phenoxy-Dioxetane Luminophores Yields Ultrasensitive Chemiluminescence Assays. Chem. Sci 2019, 10, 1380–1385. [PubMed: 30809354]

(29). Brömme HJ; Zühlke L; Silber RE; Simm A DCFH2 Interactions with Hydroxyl Radicals and Other Oxidants - Influence of Organic Solvents. Exp. Gerontol 2008, 43, 638–644. [PubMed: 18337037]

(30). Bancirova M Sodium Azide as a Specific Quencher of Singlet Oxygen during Chemiluminescent Detection by Luminol and Cypridina Luciferin Analogues. Luminescence 2011, 26, 685–688. [PubMed: 21491580]

(31). Entradas T; Waldron S; Volk M The Detection Sensitivity of Commonly Used Singlet Oxygen Probes in Aqueous Environments. J. Photochem. Photobiol. B Biol 2020, 204, No. 111787.

(32). Ruiz-González R; Zanocco AL Singlet Oxygen Fluorescent Probes. In Singlet Oxygen: Applications in Biosciences and Nanosciences; Volume 2 (2016); The Royal Society of Chemistry, 2016; 103–120.

(33). Quimby S; Fern R Novel Morphological Features of Developing Whitematter Pericytes and Rapid Scavenging of Reactiveoxygen Species in the Neighbouring Endothelia. J. Anat 2011, 219, 65–77. [PubMed: 21480891]

(34). Li RL Free Radical Biomedicine: Principles, Clinical Correlations, and Methodologies; Bentham Science Publishers, 2012.

(35). An R; Wei S; Huang Z; Liu F; Ye D An Activatable Chemiluminescent Probe for Sensitive Detection of $\gamma$-Glutamyl Transpeptidase Activity in Vivo. Anal. Chem 2019, 91, 13639–13646. [PubMed: 31560193]

(36). Taniguchi M; Lindsey JS Database of Absorption and Fluorescence Spectra of >300 Common Compounds for Use in PhotochemCAD. Photochem. Photobiol 2018, 94, 290–327. [PubMed: 29166537]

(37). Cummings BS; Wills LP; Schnellmann RG Measurement of Cell Death in Mammalian Cells. Curr. Protoc. Pharmacol 2012, 56, 12.8.1–12.8.24.

(38). Ryan LS; Gerberich J; Cao J; An W; Jenkins BA; Mason RP; Lippert AR Kinetics-Based Measurement of Hypoxia in Living Cells and Animals Using an Acetoxymethyl Ester Chemiluminescent Probe. ACS Sens. 2019, 4, 1391–1398. [PubMed: 31002225]

(39). Liu Z; Song F; Shi W; Gurzadyan G; Yin H; Song B; Liang R; Peng X Nitroreductase-Activatable Theranostic Molecules with High PDT Efficiency under Mild Hypoxia Based on a TADF Fluorescein Derivative. ACS Appl. Mater. Interfaces 2019, 11, 15426–15435. [PubMed: 30945838]

(40). Bae J; McNamara LE; Nael MA; Mahdi F; Doerksen RJ; Bidwell GL; Hammer NI; Jo S Nitroreductase-Triggered Activation of a Novel Caged Fluorescent Probe Obtained from Methylene Blue. Chem. Commun 2015, 51, 12787–12790.

(41). Sun J; Hu Z; Wang R; Zhang S; Zhang X A Highly Sensitive Chemiluminescent Probe for Detecting Nitroreductase and Imaging in Living Animals. Anal. Chem 2019, 91, 1384–1390. [PubMed: 30582678]

(42). Pitsawong W; Haynes CA; Koder RL; Rodgers DW; Miller AF Mechanism-Informed Refinement Reveals Altered Substrate-Binding Mode for Catalytically Competent Nitroreductase. Structure 2017, 25, 978–987.e4. [PubMed: 28578873]

(43). Nepali K; Lee HY; Liou JP Nitro-Group-Containing Drugs. J. Med. Chem 2019, 62, 2851–2893. [PubMed: 30295477]

(44). Sekar TV; Foygel K; Ilovich O; Paulmurugan R Noninvasive Theranostic Imaging of HSV1-Sr39TKNTR/GCV-CB1954 Dual-Prodrug Therapy in Metastatic Lung Lesions of MDA-MB-231 Triple Negative Breast Cancer in Mice. Theranostics 2014, 4, 460–474. [PubMed: 24669276]

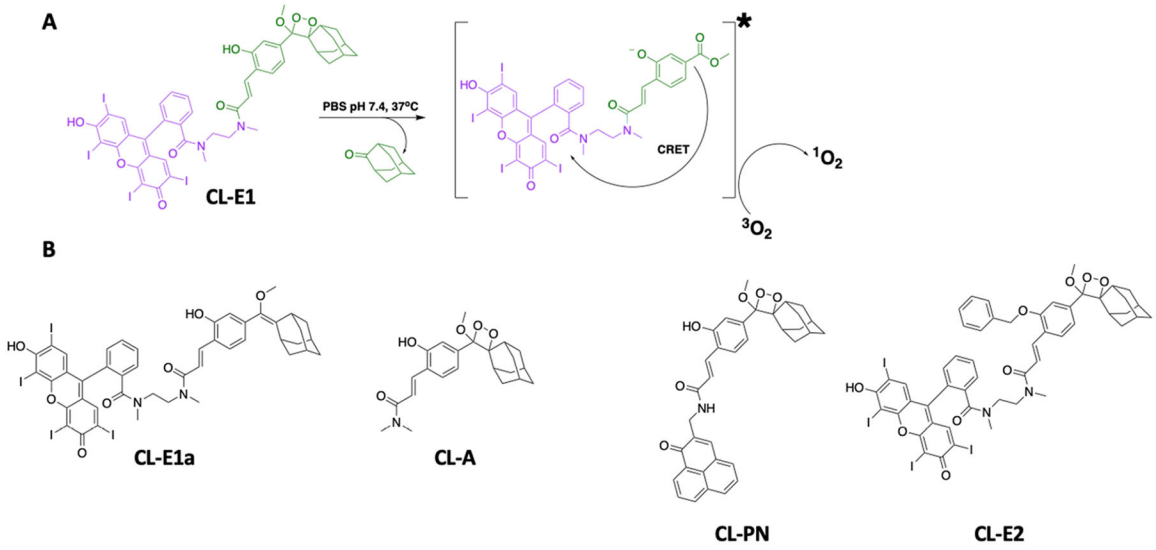


**Figure 1.**

(A) Proposed mechanism of singlet oxygen production without light excitation. The hydroxyl group on Schaap's scaffold (highlighted in green) when deprotonated in PBS pH 7.4 causes dioxetane breakdown and green chemiluminescence. Due to the close proximity of the green-absorbing photosensitizer, Erythrosin B (highlighted in purple), chemiluminescence resonance energy transfer occurs, causing Erythrosin B to produce singlet oxygen. (B) Structures of control compounds.

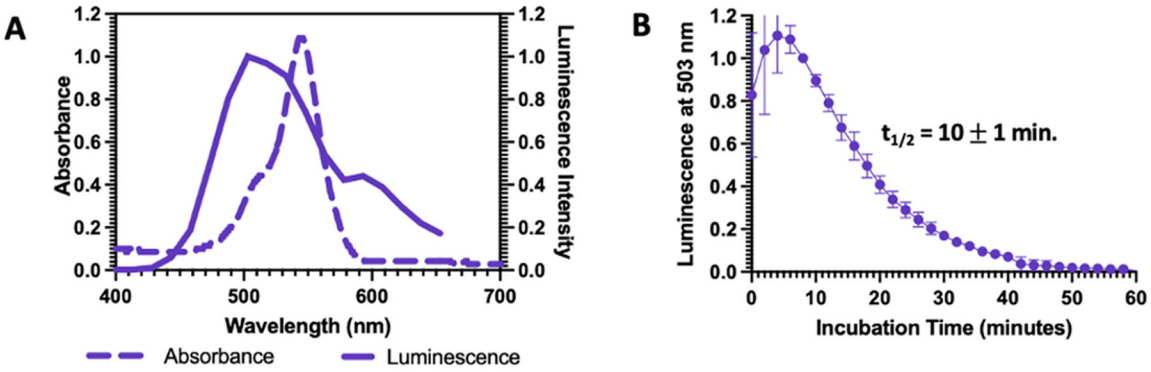


**Figure 2.**

Evidence of CRET demonstrated by luminescence and absorbance spectral comparisons and half-lives. (A) Normalized absorption spectrum of **CL-E1** (dashed line) overlayed with its normalized chemiluminescence spectrum (solid line) in PBS pH 7.4 (5% DMSO) showing that chemiluminescence resonance energy transfer is possible. (B) Chemiluminescence time course of **CL-E1** (20 $\mu$M) plotted at its luminescence wavelength maximum and normalized to 1 at the time of maximum luminescence intensity. Half-life of dioxetane breakdown was measured to be 10 ± 1 min in PBS pH 7.4 (5% DMSO). Dioxetane half-life in PBS pH 7.4 (5% DMSO) for **CL-E1** is shorter compared to control probes **CL-A** and **CL-PN** (Figure S4), suggesting that energy transfer occurs instead of energy release via luminescence. Measurements were performed in triplicate using independent samples.

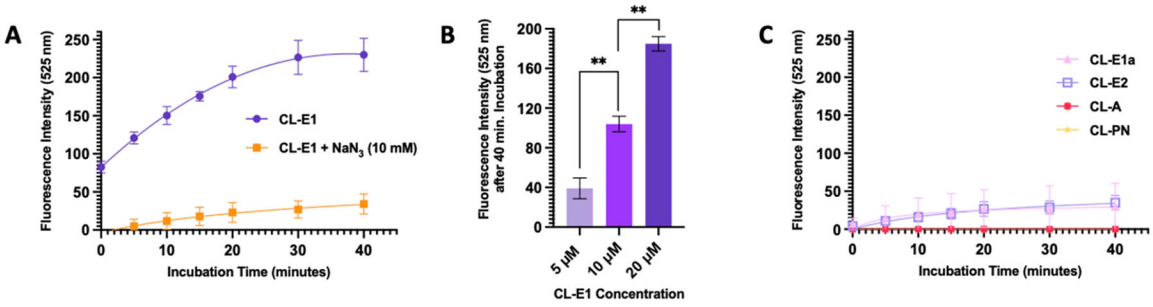


**Figure 3.**

ROS produced by (A) **CL-E1** (10 $\mu$M) in the absence (purple line) or presence (orange line) of singlet oxygen scavenger $NaN_3$ (10 mM) monitored by the fluorescence of the ROS sensor, $DCFH_2$ (5 $\mu$M), which produces the green, fluorescent product DCF upon oxidation. A higher fluorescence intensity was observed upon incubation with **CL-E1** compared to **CL-E1** in the presence of $NaN_3$. (B) Increasing concentrations of **CL-E1** were incubated with $DCFH_2$ (5 $\mu$M), where a concentration-dependent increase in DCF fluorescence was observed. Analyzed by the two-tailed *t*-test, *p*-value <0.01 indicated by **. (C) To confirm that no ROS was produced by CL control compounds, each compound at a final concentration of 10 $\mu$M was incubated with $DCFH_2$ (5 $\mu$M). A minimal increase in the fluorescence of DCF was observed for all controls. Conditions: PBS pH 7.4 (5% DMSO) at 37 °C. $\lambda_{ex}$ 490 nm. Measurements were performed in triplicate using independent samples.

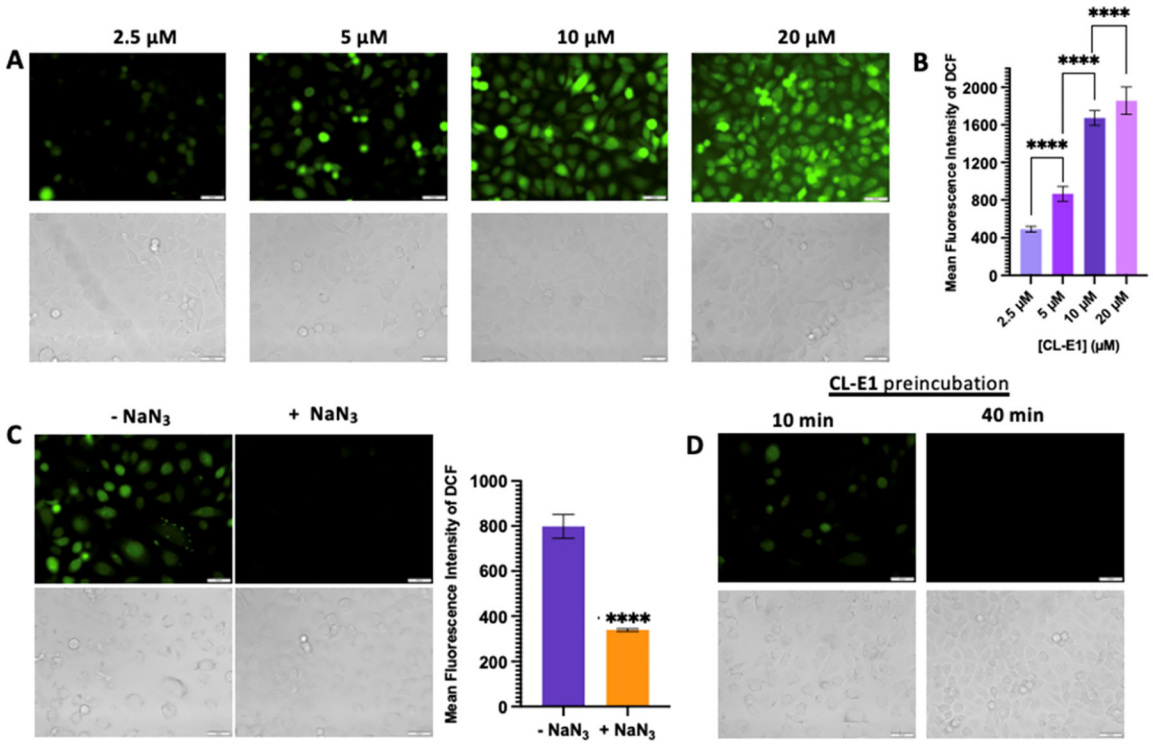


**Figure 4.**

ROS production by **CL-E1** in MCF7 breast cancer cells. (A) $DCFH_2$-DA (10 $\mu$M) with increasing concentrations of **CL-E1** (2.5–20 $\mu$M) upon 10 min incubation and washing shows a dose-dependent increase in the green fluorescence of DCF. (B) Quantification of the mean fluorescence intensity of DCF demonstrates a statistically significant increase in the ROS production by **CL-E1** at increasing concentrations. (C) Cells were incubated with the general ROS sensor, $DCFH_2$-DA (10 $\mu$M) for 30 min, followed by 10 min incubation with 5 $\mu$M **CL-E1** (left) or **CL-E1** and singlet oxygen scavenger $NaN_3$ (10 mM) (right). An increase in the green fluorescence from the ROS sensor in the presence of **CL-E1** only is indicative of ROS produced from **CL-E1** without light excitation. Quantification of the mean fluorescence intensity of DCF demonstrates the statistically significant decrease of ROS production by **CL-E1** in the presence of singlet oxygen scavenger $NaN_3$. (D) ROS production by **CL-E1** after preincubation of the dioxetane-containing probe prior to adding to MCF7 breast cancer cells. The cells were incubated with the general ROS sensor, $DCFH_2$-DA (10 $\mu$M) for 30 min, followed by addition of 5 $\mu$M **CL-E1** preincubated for 10 min (left) and 40 min (right) at 37 °C in cell culture media. Lower green fluorescence from the ROS sensor in the presence of preincubated **CL-E1** was observed, where decreased DCF signals were present for the 10 min preincubated probe, while minimal DCF signals were present for the 40 min preincubated probe—both consistent with the half-life of **CL-E1**. All images were acquired at 20×; scale bar = 50 $\mu$m. ROS sensor imaged by $\lambda_{ex}$ 470–490 nm and $\lambda_{em}$ 500–550 nm. Analyzed by the two-tailed *t*-test, *p*-value <0.0001 indicated by ****. All experiments were performed in triplicate using independent samples.

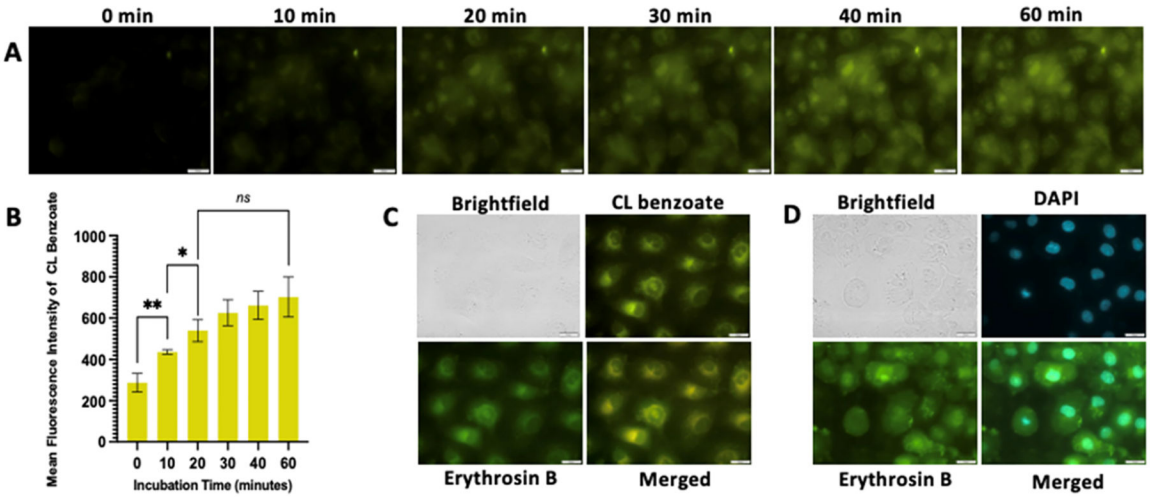


**Figure 5.**

Intracellular uptake and cellular localization of **CL-E1**. (A) Fluorescence time course of MCF7 breast cancer cells incubated with 10 $\mu$M **CL-E1** for a total of 60 min. The benzoate ester product expected produces yellow fluorescence upon excitation ($\lambda_{ex}$ 400 nm) with increasing fluorescence up to maximum signals between 20 and 40 min of incubation with **CL-E1**. (B) Quantification of the mean fluorescence intensity for the benzoate ester product. Data for 0 min incubation represent the cells imaged immediately after addition of **CL-E1**. Analyzed by the two-tailed *t*-test, *p*-value <0.0001 indicated by ****, *p*-value = 0.0076 indicated by **, and *p*-value >0.05 is not significant. (C) MCF7 breast cancer cells incubated with 10 $\mu$M **CL-E1** for 20 min. The benzoate ester product expected produces yellow fluorescence (top right) upon excitation ($\lambda_{ex}$ 400 nm), and the attached photosensitizer Erythrosin B to the CL scaffold shows green fluorescence (bottom left) ($\lambda_{ex}$ 509 nm). Yellow fluorescence and green fluorescence overlay well with each other (bottom right), demonstrating the same cellular localization. (D) Nuclear costain with DAPI (5 $\mu$M) (top right) overlayed (bottom right) with green fluorescence from Erythrosin B (bottom left). Additional imaging of the benzoate ester with nuclear costain is not feasible due to the excitation and emission properties interfering with those of DAPI. 40×, scale bar = 25 $\mu$m. Experiments were performed in triplicate using independent samples.

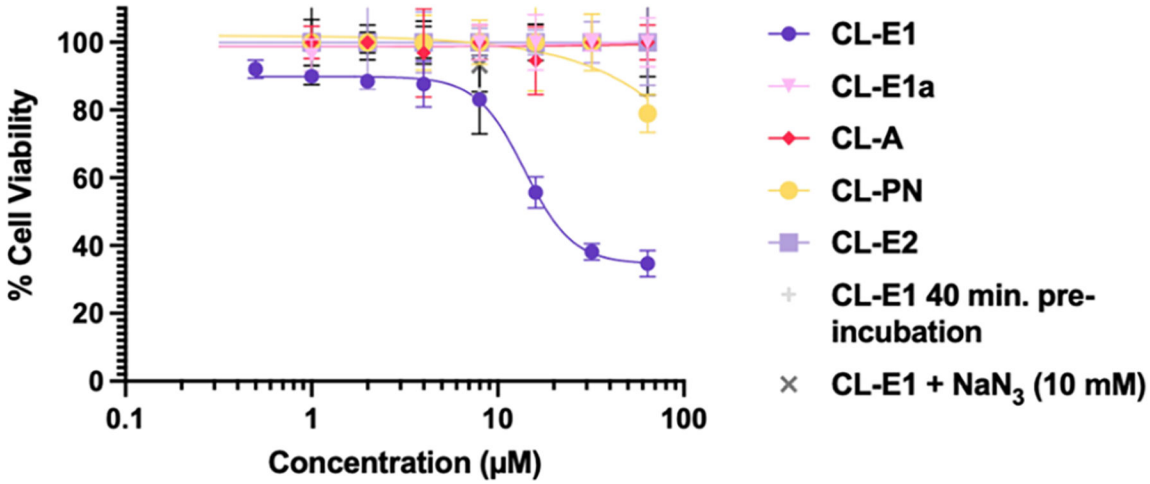


**Figure 6.**

Cell viability of MCF7 cells. **CL-E1**-treated cells produce a dose response on viability (relative $IC_{50}$ 14 ± 2 $\mu$M) but not in the presence of the singlet oxygen quencher $NaN_3$ or if preincubated for 40 min prior to adding to MCF7 cells. Controls lacking dioxetane, Erythrosin B, and a free phenol showed minimal cell death compared to **CL-E1**. All compounds were incubated with MCF7 cells overnight and then assayed for viability using an MTT assay. Experiments were performed in triplicate.

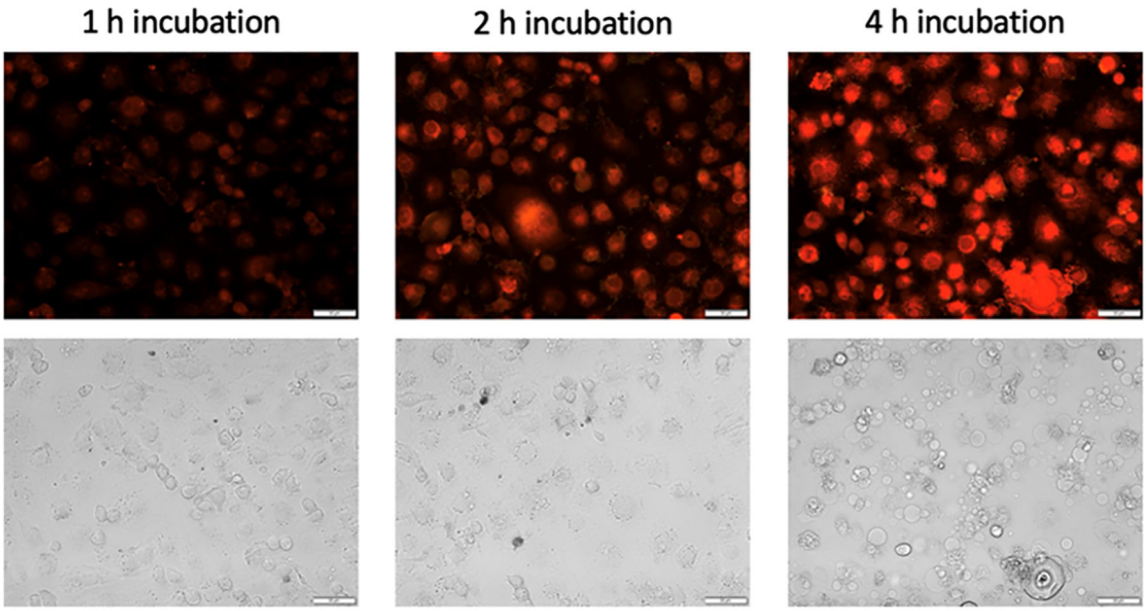


**Figure 7.**

Mechanism of cell death induced by **CL-E1** in MCF7 breast cancer cells was determined by incubating cells with 32 $\mu M$ **CL-E1**, followed by the addition of cell death indicators Annexin V-FITC and propidium iodide (PI), which were used to differentiate between apoptotic cells and necrotic cells, respectively. Only red fluorescent signals from PI were observed when overlayed with the fluorescence image of Annexin V-FITC, with a time-dependent increase in red fluorescence and nuclear signals being most prominent after 4 h incubation with **CL-E1**, suggesting that necrosis is the mechanism of cell death induced. 20×, scale bar = 50 $\mu$m. Annexin V-FITC imaged by $\lambda_{ex}$ = 470–490 nm and $\lambda_{em}$ = 500–550 nm and PI imaged by $\lambda_{ex}$ = 505–555 nm and $\lambda_{em}$ = 600–700 nm. Experiments were performed in triplicate using independent samples.

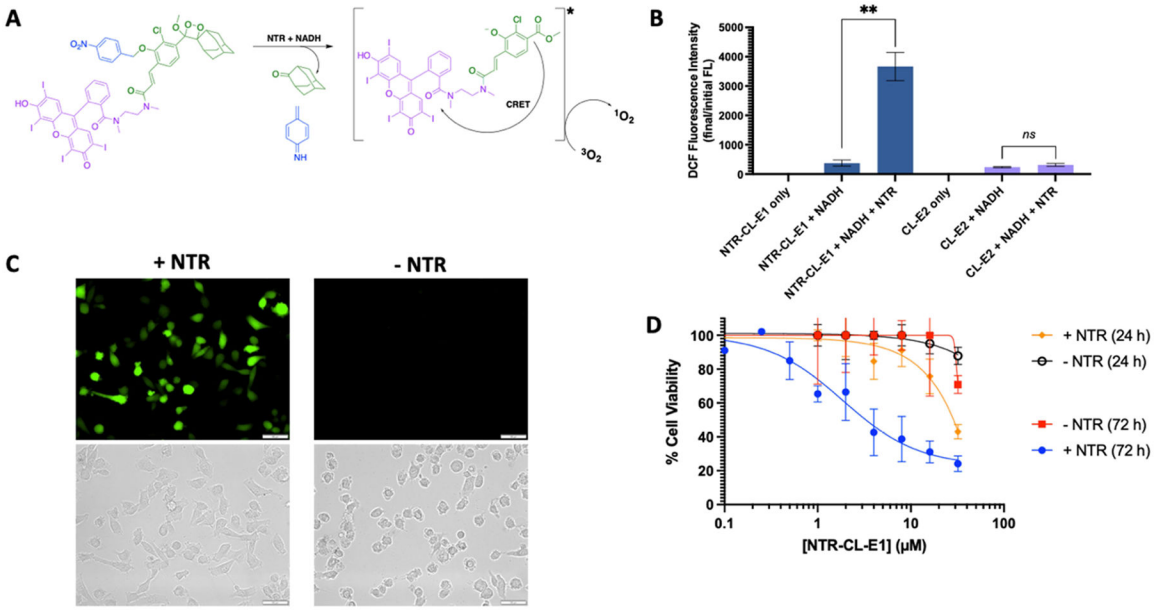


**Figure 8.**

(A) Proposed mechanism of NTR activation toward **NTR-CL-E1**. NTR reduces the nitro group on the 4-nitrobenzyl trigger group in the presence of NADH, releasing the CL scaffold with a free phenol, followed by dioxetane breakdown and energy transfer to the photosensitizer, Erythrosin B, for singlet oxygen production. (B) ROS production by 10 $\mu$M **NTR-CL-E1** (blue) or **CL-E2** (purple), after overnight incubation in the presence of NADH (200 $\mu$M) with or without NTR (1.5 $\mu$M) (blue). ROS observed for **NTR-CL-E1** and not **CL-E2**. Analyzed by the two-tailed *t*-test, *p*-value <0.01 indicated by **. Conditions: PBS pH 7.4 (5% DMSO) at 37 °C. $\lambda_{ex}$ 490 nm. (C) ROS production by **NTR-CL-E1** in MDA-MB231 triple negative breast cancer cells +/− NTR expression. The cells were incubated with **NTR-CL-E1** (10 $\mu$M) for 15 min, followed by the addition of the general ROS sensor, $DCFH_2$-DA (10 $\mu$M) for an additional 30 min (45 min total incubation with **NTR-CL-E1**). An increase in the green fluorescence from the oxidized ROS sensor (DCF) in the presence of **NTR-CL-E1** was only present in cells expressing NTR. 20×, scale bar = 50 $\mu$m. ROS sensor imaged by $\lambda_{ex}$ 470–490 nm and $\lambda_{em}$ 500–550 nm. (D) Incubation of **NTR-CL-E1** in MDA-MB231 triple negative breast cancer cells +/− NTR expression demonstrates dose-dependent cytotoxicity in cells only expressing NTR after 24 h and after 72 h incubation ($IC_{50}$ = 1.9 ± 0.7 $\mu$M). Measurements were performed in triplicate.